Learning a Unified Policy for Whole-Body Control of Manipulation and Locomotion

Anonymous Author(s)
Affiliation
Address
email

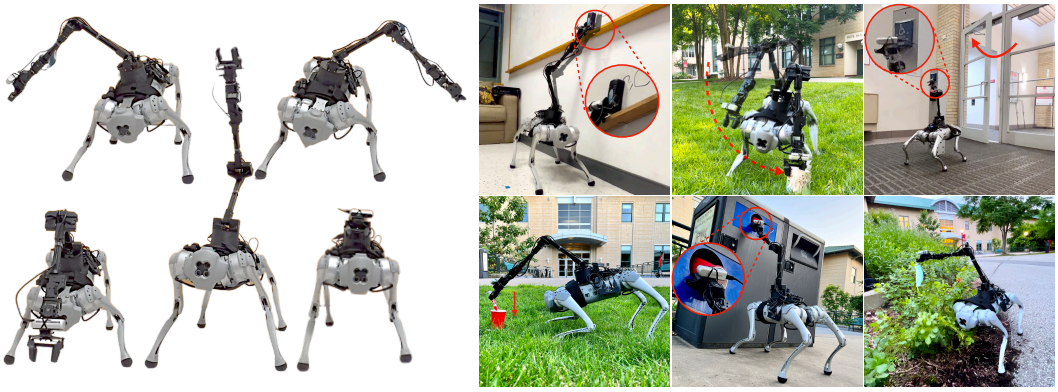

Figure 1: We present a framework for whole-body control of legged robots with robotic arm. Left shows how whole-body coordination achieves larger workspace by bending and stretching of legs. Right half shows different real-world tasks, including wiping whiteboard, picking up a cup, pressing door-open button, placing, throwing a cup into a garbage bin and picking in clustered environments. Videos at https://maniploco.github.io/

Abstract: An attached arm can significantly increase the applicability of legged robots to several mobile manipulation tasks that are not possible for the wheeled or tracked counterparts. The standard learning paradigm for such legged manipulators is to decouple the problem into that of manipulation and locomotion. However, this is ineffective and requires immense engineering to support coordination between arm and legs, error can propagate across modules, and causes non-smooth unnatural motions. This is also biological implausible where there is evidence for strong motor synergies across limbs. In this work, we propose to learn a unified whole-body control for a legged manipulator using reinforcement learning. We follow advantage mixing using the causal dependency in the action space to get around the local minima and difficulty in training the joint system. We also propose a simple design for a low-cost legged manipulator and find that our unified policy can demonstrate dynamic and agile behaviors across several task setups. Videos are at https://maniploco.github.io/

Keywords: Mobile Manipulation, Whole-Body Control, Legged Locomotion

1 Introduction

Locomotion has seen impressive performance in the last decade with results in challenging outdoor and indoor terrains, otherwise unreachable by their wheeled or tracked counterparts. However, there are strong limitations to what a legged-only robot can achieve since, besides visual inspection, even the most basic everyday tasks require some form of manipulation. This has led to immense progress in general-purpose legged manipulators primarily achieved through physical modeling of dynamics [1, 2, 3, 4, 5, 6]. However, modeling a legged robot with attached arm is a dynamic, high-dimensional, and non-smooth control problem, requiring substantial domain expertise and engineering effort on the part of the designer. The control frameworks are often hierarchical with

Submitted to the 6th Conference on Robot Learning (CoRL 2022). Do not distribute.

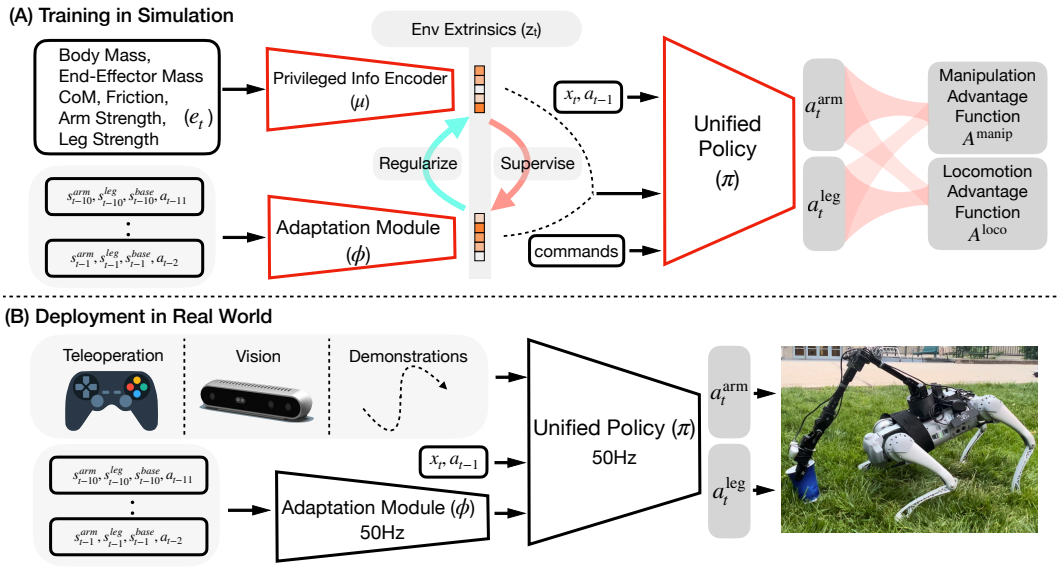

Figure 2: Whole-body control framework. During training, a unified policy is learned by conditioned on environment extrinsics. During deployment, the adaptation module is reused without any real-world fine-tuning. The robot can be commanded in various modes including teleoperation, vision and open-loop control.

simplified models at higher levels [7], thus limited to operating in constrained settings. Hence, there has been increasing interest in approaching this problem via reinforcement learning (RL) which could help lower the engineering burden while being able to generalize to diverse scenarios.

However, most learning approaches for legged mobile manipulators [8] have also followed their control counterparts [9, 10] in treating the problem as a hybrid system to train decoupled controllers for the legs and arm. This is ineffective due to several practical reasons including lack of coordination between arm and legs, error propagation across modules, slow, non-smooth and unnatural motions. Furthermore, it is far from the whole-body motor control in humans where studies suggest strong coordination between limbs. In fact, the control of hands and legs is so tied together that they form low-dimension synergies, as outlined over 70 years ago in a seminal series of writings by Russian physiologist Nikolai Bernstein [11, 12, 13]. Perhaps the simplest example is how it is hard for humans to move one arm and the corresponding leg in different motions while standing. A whole-body control not only allows coordination but also extends the capabilities of the individual parts. For instance, our robot bends or stretches its legs with the movement of the arm to extend the reach of the end-effector as shown in Figure 1. But, people move in order to manipulate and interact with environments, so we need the ability to manipulate on top of moving.

However, unlike legged locomotion, it is not straightforward to scale the standard RL paradigm of training the policies in simulation and then transfer to the real world due to several challenges with whole-body control. (a) *High-dimensional control*: Our robot shown in Figure 3 has total 19 degrees of freedom. This problem is exacerbated in legged manipulators because the control is dynamic, continuous and high-frequency leading up to an exponentially large search space even in few seconds of trajectory. (b) *Conflicting policies and local minima*: Consider when the arm tilts to the right, the robot needs to change the walking gait to account for the weight balance. This curbs the locomotion abilities and makes training prone to learn only one of either locomotion or manipulation well. (c) *Dependency*: Consider picking an object on the ground, the end-effector of the arm needs support from the torso by bending legs. This means the absolute performance of manipulation is bounded until legs can adapt.

In this work, we present both a hardware setup for low-cost legged manipulators and a method for learning one single policy to control and coordinate both legs and arm, which is compatible with diverse operating modes, and successfully deploy it on a customized budget fully untethered hardware setup as shown in Figure 1. The key insights of the method are that we can exploit the causal structure

	Command Following	Energy	Alive
r^{loco}	$-0.5 * \lvert v_x - v_x^{\text{cmd}} \rvert + 0.15 \cdot e^{-\lvert \omega_{\text{yaw}} - \omega_{\text{yaw}}^{\text{cmd}} \rvert}$	$-0.00005 \cdot \sum_{i \in \text{leg joints}} \lvert \tau_i \dot{q}_i \rvert^2$	$0.2 + 0.5 \cdot v_x^{\text{cmd}}$
r^{manip}	$0.5 \cdot e^{-\lVert [p,o] - [p^{\text{cmd}}, o^{\text{cmd}}] \rVert_1}$	$-0.004 \cdot \sum_{j \in \text{arm joints}} \lvert \tau_j \dot{q}_j \rvert$	0

Table 1: Both locomotion and manipulation rewards follow: $r_{\text{tracking}} + c * r_{\text{energy}} + r_{\text{alive}}$, which encourages command following while penalizes positive mechanical energy consumption to enable smooth motion [17]. Denote forward base linear velocity v_x, yaw angular base velocity ω_{yaw}, torque τ, joint angle velocity $\dot{q}$.

in action space with respect to manipulation and locomotion to stabilize and speed up learning, and adding regularization to domain adaptation bridges the gap between simulation with full states and real world with only partial observations.

We perform evaluation on our proposed legged manipulator. Despite immense progress, there exists no easy to use legged manipulator for academic labs. Most publicized robot is Spot Arm from Boston Dynamics [14], but the robot comes with pre-designed controllers that can be changed. Another example is the ANYmal robot with custom arm [8] from ANYbotics. Notably, both these hardware setups are expensive (more than 100K USD). We implement a simple design of low-cost legged Go1 robot [15] with low-cost arm on top. Our legged manipulator can run fully untethered with modest on-board compute. We show the effectiveness of our learned whole-body controller for teleoperation, vision-guided control as well as open-loop control setup across tasks such as picking objects, throwing garbage, pressing buttons on walls etc. Our robot exhibits **dynamic** and **agile** leg-arm coordinated motions as shown in the video at `https://maniploco.github.io/`.

2 Method: A Unified Policy for Coordinated Manipulation and Locomotion

We formulate the unified policy π as one neural network where the inputs are current base state $s_t^{\text{base}} \in \mathbb{R}^5$ (row, pitch, and base angular velocities), arm state $s_t^{\text{arm}} \in \mathbb{R}^{12}$ (joint position and velocity of each arm joint), leg state $s_t^{\text{leg}} \in \mathbb{R}^{28}$ (joint position and velocity of each leg joint, and foot contact indicators), last action $a_{t-1} \in \mathbb{R}^{18}$, end-effector position and orientation command $[p^{\text{cmd}}, o^{\text{cmd}}] \in \mathbb{SE}(3)$, base velocity command $[v_x^{\text{cmd}}, \omega_{\text{yaw}}^{\text{cmd}}]$, and environment extrinsics $z_t \in \mathbb{R}^{20}$ (details in Section 2.2). The policy outputs target arm joint position $a_t^{\text{arm}} \in \mathbb{R}^6$ and target leg joint position $a_t^{\text{arm}} \in \mathbb{R}^{12}$, which are subsequently converted to torques using PD controllers. We use joint-space position control for both legs and the arm. As opposed to operational space control of the arm, joint-space control enables learning to avoid self-collision and smaller Sim-to-Real gap, which is also found to be useful in other setups involving multiple robot parts, like bimanual manipulation [16].

We use RL to train our policy π by maximizing the discounted expected return $\mathbb{E}_\pi \left[\sum_{t=0}^{T-1} \gamma^t r_t \right]$, where r_t is the reward at time step t, γ is the discount factor, and T is the maximum episode length. The reward r is the sum of manipulation reward r^{manip} and locomotion reward r^{loco} as shown in Table 1. Notice that we use the second power of energy consumption at each leg joint to encourage both lower average and lower variance across all leg joints.

Command Vars	Training Ranges	Test Ranges
v_x^{cmd}	[0, 0.9]	[0.8, 1.0]
$\omega_{yaw}^{\text{cmd}}$	[-1,0, 1.0]	[-1, -.7] & [.7, 1]
l	[0.2, 0.7]	[0.6, 0.8]
p	$[-2\pi/5, 2\pi/5]$	$[-2\pi/5, 2\pi/5]$
y	$[-3\pi/5, 3\pi/5]$	$[-3\pi/5, 3\pi/5]$
T_{traj}	[1, 3]	[0.5, 1]

Table 2: Ranges for uniform sampling of command variables

We parameterize the end-effector position command p^{cmd} in spherical coordinate (l, p, y), where l is the radius of the sphere and p and y are the pitch and yaw angle. The origin of the spherical coordinate system is set at the base of the arm. We set the end-effector pose command p^{cmd} by interpolating between the current end-effector position p and a randomly sampled end-effector position p^{end} every T_{traj} seconds:

Env Params	Training Ranges	Test Ranges
Base Extra Payload	[-0.5, 3.0]	[5.0, 6.0]
End-Effector Payload	[0, 0.1]	[0.2, 0.3]
Center of Base Mass	[-0.15, 0.15]	[0.20, 0.20]
Arm Motor Strength	[0.7, 1.3]	[0.6, 1.4]
Leg Motor Strength	[0.9, 1.1]	[0.7, 1.3]
Friction	[0.25, 1.75]	[0.05, 2.5]

Table 3: Ranges for uniform sampling of environment parameters

$$p_t^{\text{cmd}} = \frac{t}{T_{\text{traj}}} p + \left(1 - \frac{t}{T_{\text{traj}}}\right) p^{\text{end}}, \; t \in [0, T_{\text{traj}}].$$

p^{end} is resampled if any p_t^{cmd} leads to self-collision or collision with the ground. o^{cmd} is uniformly sampled from $\mathbb{SO}(3)$ space. Table 2 lists the ranges for sampling of all command variables.

2.1 Advantage Mixing for Policy Learning

Training a robust policy for a high-DoF robot is hard. In both manipulation and locomotion learning literature, researchers have used curriculum learning to ease the learning process by gradually increasing the difficulty of tasks so that the policy can learn to solve simple tasks first and then tackle difficult tasks [18, 19, 20]. However, most of these works require many manual tunings of a diverse set of the curriculum parameters and careful design of the mechanism for automatic curriculum.

Instead of introducing a large number of curricula on the learning and environment setups, we relies on only one curriculum with only one parameter to expedite the policy learning. Since we know that manipulation tasks are mostly related to the arm actions and locomotion tasks largely depends on leg actions, we can formulate this inductive bias in policy optimization by mixing advantage functions for manipulation and locomotion to speed up policy learning. Formally, for a policy with diagonal Gaussian noise and a sampled transition batch D, the training objective with respect to policy's parameters θ_π is

$$J(\theta_\pi) = \frac{1}{|\mathcal{D}|} \sum_{(s_t,a_t)\in\mathcal{D}} \log \pi(a_t^{\text{leg}} \mid s_t) \left(A^{\text{loco}} + \beta A^{\text{manip}}\right) + \log \pi(a_t^{\text{arm}} \mid s_t) \left(\beta A^{\text{loco}} + A^{\text{manip}}\right)$$

β is the curriculum parameter that linearly increases from 0 to 1 over timesteps T_{mix}: $\beta = \min(t/T_{\text{mix}}, 1)$. A^{manip} and A^{loco} are advantage functions based on r^{manip} and r^{loco} respectively. Intuitively, the advantage mixing reduces the credit assignment complexity by first attributing difference in manipulation returns to arm actions and difference in locomotion returns to leg actions, and then gradually anneal the weighted advantage sum to encourage learning arm and leg actions that help locomotion and manipulation respectively. We optimize this RL objective by PPO [21].

2.2 Regularized Online Adaptation for Sim-to-Real Transfer

Many prior works on Sim-to-Real transfer utilize the two-phase teacher-student scheme to first train a teacher network by RL using privileged information that is only available in simulation, and then the student network using onboard observation history imitates the teacher policy either in explicit action space or latent space [22, 23, 24, 25]. Due to the information gap between the full state available to the teacher network and partial observability of onboard sensories, the teacher network may provide supervision that is impossible for the student network to predict, resulting in an imitation gap. This problem is also noted in Embodied AI community [26]. In addition, the second phase can only starts after the convergence of the first phase, which creates extra burdens for both training and deployment.

To tackle the imitation gap and to remove the two-phase pipeline, we propose Regularized Online Adaptation (shown in Figure 2). Concretely, the encoder μ takes the privileged information e as input and predict an enviornment extrinsics latent z^μ for the unified policy to adapt its behavior in different environments. The adaptation module ϕ estimates the environment extrinsics latent z^ϕ by only condition on recent observation history from robot's onboard sensories. We jointly train μ with the unified policy π end-to-end by RL and regularize z^μ to avoid large deviation from z^ϕ estimated by the adaptation module. The adaption module ϕ is trained by imitating z^μ online. We formulate the loss function of the whole learning pipeline with respect to policy's parameters θ_π, privileged information encoder's parameters θ_μ, and adaptation module's parameters θ_ϕ as

$$L(\theta_\pi, \theta_\mu, \theta_\phi) = -J(\theta_\pi, \theta_\mu) + \lambda||z^\mu - \text{sg}[z^\phi]||_2 + ||\text{sg}[z^\mu] - z^\phi||_2 \ ,$$

where $J(\theta_\pi, \theta_\mu)$ is the RL objective discussed in Section 2.1, $\text{sg}[\cdot]$ is the stop gradient operator, and λ is the Laguagrian multiplier. The loss function can be minimized by using dual gradient descent: $\theta_\pi, \theta_\mu \leftarrow \arg\min_{\theta_\pi,\theta_\mu} \mathbb{E}_{(s,a)\sim\pi(\ldots,z^\mu)}[L]$, $\theta_\phi \leftarrow \arg\min_{\theta_\phi} \mathbb{E}_{(s,a)\sim\pi(\ldots,z^\phi)}[L]$, and $\lambda \leftarrow \lambda + \alpha\frac{\partial L}{\partial \lambda}$ with step size α. This optimization process is known to converge [27, 28]. In practice, we alternate the optimization process of the unified policy π and encoder μ and the one of adaptation module ϕ by a fixed number of gradient steps. λ increases from 0 to 1 by a fixed linear scheme. Notice that [22] is a special case of Regularized Online Adaptation which sets λ to be constant zero and ϕ starts training only after training convergence of π and μ.

	Survival ↑	Base Accel. ↓	Vel Error ↓	EE Error ↓	Tot. Energy ↓
Unified (Ours)	**97.1** ± 0.61	**1.00** ± 0.03	**0.31** ± 0.03	**0.63** ± 0.02	50 ± 0.90
Separate	92.0 ± 0.90	1.40 ± 0.04	0.43 ± 0.07	0.92 ± 0.10	51 ± 0.30
Uncoordinated	94.9 ± 0.61	1.03 ± 0.01	0.33 ± 0.01	0.73 ± 0.02	**50** ± 0.28

Table 4: Comparison of unified policy with separate policies for legs-arm, and one uncoordinated policy. The unified policy achieves the best performance given same energy consumption. The test ranges are in Table 2.

Deployment During deployment, the unified policy and adaptation module executes jointly onboard. To specify commands, we develop three interfaces: teleopertion by joysticks, closed-loop control by using RGB tracking, and open-loop reply of human demonstrations. Details are in Section 3.3.

3 Experimental Results

3.1 Robot System Setup

The robot platform is comprised of a Unitree Go1 quadraped [15] with 12 actuatable DoFs, and a robot arm which is the 6-DoF Interbotix WidowX 250s [29] with a parallel gripper. We mount the arm on top of the quadruped. The RealSense D435 provides RGB visual information and is mounted close to the gripper of WidowX. Both power of Go1 and WidowX are provided by Go1's onboard battery. Neural network inference is also done onboard of Go1. Our robot system uses only onboard computation and power so it is fully untethered.

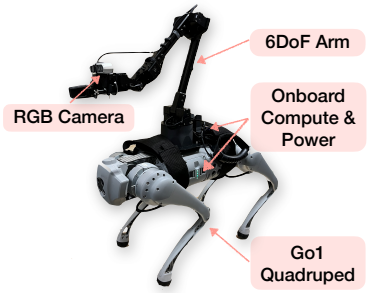

Figure 3: Robot system setup

3.2 Simulation Experiments

The purpose of our simulation experiments is to address the following questions:

- Does the unified policy improves over separate policies for the arm and legs? If so, how?
- How advantage mixing helps learning the unified policy?
- What's the performance of Regularized Online Adaptation compared with other Sim2Real methods?

Baselines and Metrics: We compare our method with the following baselines:

1. Separate policies for legs and the arm: one policy controls legs based on the quadraped observation, and another policy controls the arm based on arm observation.
2. One uncoordinated policy: Same as unified policy which observes aggregate state of base, legs and the arm, but only r^{manip} is used to train arm actions, and only r^{loco} for leg actions.
3. Rapid Motor Adaptation (RMA) [22]: same as Regularized Online Adaptation when the regularization coefficient λ is a constant zero.
4. Expert policy: the unified policy using the privileged information encoder z^{μ}.
5. Domain Randomization: the unified policy trained without environment extrinsics z.

We report following metrics: (1) survival percentage, (2) Base Accel: angular acceleration of base, (3) Vel Error: L1 error between base velocity commands and actual base velocity, (4) EE Error: L1 error between EE command and actual EE pose, (5) Tot. Energy: total energy consumed by legs and the arm. All metrics are normalized by episode length. All experiments are tested over 3 randomly initialized networks and 1000 episodes each. Details of simulation and training are in Supplementary.

Improvements of the Unified Policy over Baselines: In Table 4, our unified policy outperforms separate and uncoordinated policies because both the arm and leg actions are trained with the sum of reward for manipulation and locomotion and are given with observations for the arm, legs and the quadraped base, while baselines struggle to maintain a small base acceleration, which results in larger error in command velocity tracking and inaccurate EE pose tracking.

Unified Policy Increases Whole-body Coordination: Table 5 shows that our unified policy promotes whole-body coordination where (1) leg actions will help the arm to achieve a larger workspace via bending for lower EE commands

	Arm workspace (m^3) ↑	Survival under perturb ↑
Unified (Ours)	**0.82** ± 0.02	**0.87** ± 0.04
Separate	0.58 ± 0.10	0.64 ± 0.06
Uncoordinated	0.65 ± 0.02	0.77 ± 0.06

Table 5: In unified policy, legs help increase the arm workspace and the arm helps the quadruped to stabilize.

	Imitation Error $\|z^\mu - z^\phi\|_2$ ↓	Survival ↑	Base Accel. ↓	Vel Error ↓	EE Error ↓	Tot. Energy ↓
Domain Randomization	-	95.8 ± 0.2	**0.44** ± 0.00	0.46 ± 0.00	0.40 ± 0.00	**21.9** ± 0.53
RMA [22]	0.31 ± 0.01	95.2 ± 0.2	0.54 ± 0.02	0.44 ± 0.00	0.26 ± 0.04	27.3 ± 0.95
Regularized Online Adapt (Ours)	**2e-4** ± 0.00	**97.4** ± 0.1	0.51 ± 0.02	**0.39** ± 0.01	**0.21** ± 0.00	25.9 ± 0.56
Expert w/ Reg.	-	97.8 ± 0.2	0.52 ± 0.02	0.40 ± 0.01	0.21 ± 0.00	25.8 ± 0.49
Expert w/o Reg.	-	98.3 ± 0.2	0.51 ± 0.02	0.39 ± 0.00	0.21 ± 0.00	25.6 ± 0.30

Table 6: Regularized Online Adaptation outperforms other baselines with the smallest imitation error which helps it to have the same performance as the expert policy which uses privileged information to predict environment extrinsics. Expert policy trained with regularization term $\|z^\mu - \text{sg}[z^\phi]\|_2$ has negligible performance degradation compared with the expert trained without regularization. Test ranges in Table 3. Domain Randomization learns to just stand in most cases, hence, trivially collapsing to low Tot. Energy and Base Accel.

and standing up high for higher EE commands, and (2) arm will help the robot balance under larger perturbation (1.0 m/s initial velocity of base) resulting in higher survival rate of the unified policy. We estimate the the arm workspace via calculating the volume of the convex hull of 1000 sampled EE poses, subtracted by the volume of a cube that encloses the quadruped.

Advantage Mixing Helps Learning the Unified Policy: Without Advantage Mixing, the unified policy has difficulty in credit assignment, resulting in the policy first learns EE tracking but ignores the locomotion task. As shown in Figure 4, Advantage Mixing helps the policy to focus on each task first and then merge them together, which induces a curriculum-like mechanism to speed up training. Details in Supplementary.

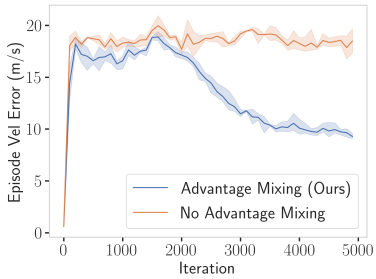

Figure 4: Advantage mixing helps the unified policy to learn to follow the command velocity much faster (aggregated Vel Error over episodes decreases sharply) than without mixing.

Robust OOD Performance of Regularized Online Adaptation: We find that our Regularized Online Adaptation is more robust than RMA and Domain Randomization (DR). In RMA, it is not guaranteed the estimated environment extrinsics by the adaptation module can imitates the one learned by the expert. With Regularized Online Adaptation, the expert learns to predict environment extrinsics with regularization from the adaptation module, thus tiny imitation error, **resulting in 20% reduction in EE Error**. Table 6 shows that adding regularization to expert has negligible negative impact on performance, while every metric gets improved compared to RMA due to smaller latent imitation error. Note that DR has better base acceleration and total energy as it just stands in place under difficult environments.

3.3 Real-World Experiments

We use the decoupled default Go1 MPC controller and the IK solver for operational space control of WidowX as the baseline in the real world, which we refer to as MPC+IK.

Teleoperation: In simulation, a random end point p^{end} is sampled and subsequent interpolation produces a trajectory for the end-effector to follow. In the real world, we only need to specify p_t^{cmd} without worrying about p^{end}. We parameterize $p_{t+1}^{\text{cmd}} = p_t^{\text{cmd}} + \Delta p$, where $\Delta p = (\Delta l, \Delta p, \Delta y)$ is from joystick. With human in the loop, we can command the end-effector to reach points within or outside training distribution. By teleoperating the robot, we collect real-world data to show how the quadruped and the arm coordinate. In Figure 5, we analyze how the end-effector goal command p_t^{cmd} relates to the quadruped's base rotation $(r^{\text{quad}}, p^{\text{quad}}, y^{\text{quad}})$.

Vision-Guided Tracking: In addition to joystick control by humans, we also show successful picking tasks using sole visual feedback from an RGB camera. We mount a Realsense D435i camera near the gripper of the arm and use AprilTag [30] to get the relative position between the gripper and the object to be picked up. AprilTag is a visual fiducial system popular in robotics research using simple 2D black and white blocks to encode pose information. First we get the translation of the AR tag in the camera frame $p_{\text{tag}} = [x_{\text{tag}}, y_{\text{tag}}, z_{\text{tag}}]^T$. Then we design and use a simple yet effective position feedback controller to command the end-effector to the desired position, where we set current end-effector position $p_t^{\text{cmd}} = K^T p_{\text{tag}}$, where $K = [-1.5, -1.5, 0.1]^T$ is a gain vector for position control. We initialize the robot to the same initial configuration and use vision feedback

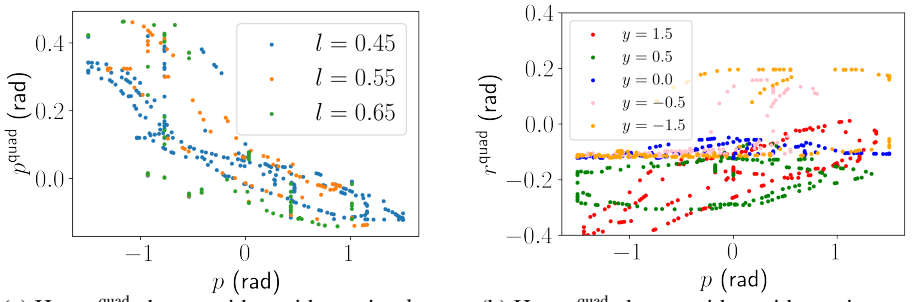

(a) How p^{quad} change with p with varying l. (b) How r^{quad} change with p with varying y.

Figure 5: Coordination through teleoperation. (a) We fix $y = 0$ and change p and l, we can see that when p has a large absolute value, the quadruped will pitch up or down to help the arm reach for its goal. With larger l (further goal), the quadruped will pitch harder to help. (b) When the absolute value of y is closer to 1.578 (arm turns to the side of the robot), the quadruped will roll more to help the arm. When $y = 0$, there is no roll because in this scenario the quadruped needs to pitch down instead of rolling to help the arm.

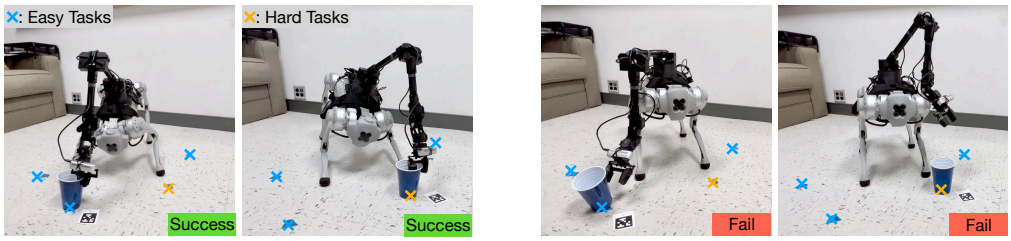

(a) Our method succeed in both easy and hard tasks with coordinated behaviors.

(b) MPC+IK fails both tasks. Left: fail due to missed cup. Right: failure due to self collision.

Figure 6: Comparison of our method versus baseline controller in vision feedback pick-up tasks. We sample different point around the robot as the target pick-up position. 3 points are in normal distance from the robot, which we define as easy tasks. There is one point that is very close to the robot's front left foot and is hard to reach without coordination, which we define as hard task. One easy task and one hard task are shown.

to grasp a cup at various positions as shown in Figure 6. Our method has high success rate due to coordinated behavior between quadruped and the arm. For MPC+IK, the quadruped does not move while the arm is moving and has low success rate in both tasks.

Failure Mode Analysis: Our method succeeds most of times on easy tasks without visible performance drop in hard task, see Table 7. The failed trials of our method are largely due to the mismatch between the actual cup position and the AR tag position. Since the visual estimation is not the focus of this work, we infer that our method has high precision and high efficiency on pick-up tasks compared to MPC+IK. MPC+IK succeeds some of the easy tasks and fails due to IK singularity or self-collision with quadruped body. In hard tasks, the major failure cause is self-collision given the cup is too close to the body. Notice that the TTC of MPC+IK is also longer than our method because solving online IK and operational space control is compute-demanding for on-board compute.

	Ground Points (p^{end})	Success Rate ↑	TTC ↓	IK Failure Rate ↓	Self Collision Rate ↓
Easy scenario (tested on 3 points)					
Ours	$\begin{bmatrix}(0.62, -1.27, -1.11)\\(0.57, -1.16, 0.55)\\(0.58, -1.14, 1.78)\end{bmatrix}$	**0.8**	**5s**	-	**0**
MPC+IK		0.3	17s	0.4	0.3
Hard scenario (tested on 1 point)					
Ours	(0.55, -0.75, -0.43)	**0.8**	**6s**	-	**0**
MPC+IK		0	∞	0.2	0.8

Table 7: Comparison of our method v.s. MPC+IK on pick-up tasks. p^{end} is the goal position sampled from the points on the ground. TTC is the average time to tompletion. All data are averaged on 10 real-world trials.

Open-loop Control from Demonstration: In this part, we analyze how dynamic walking is coupled with whole-body coordination. The robot is given a pre-defined end-effector trajectory to

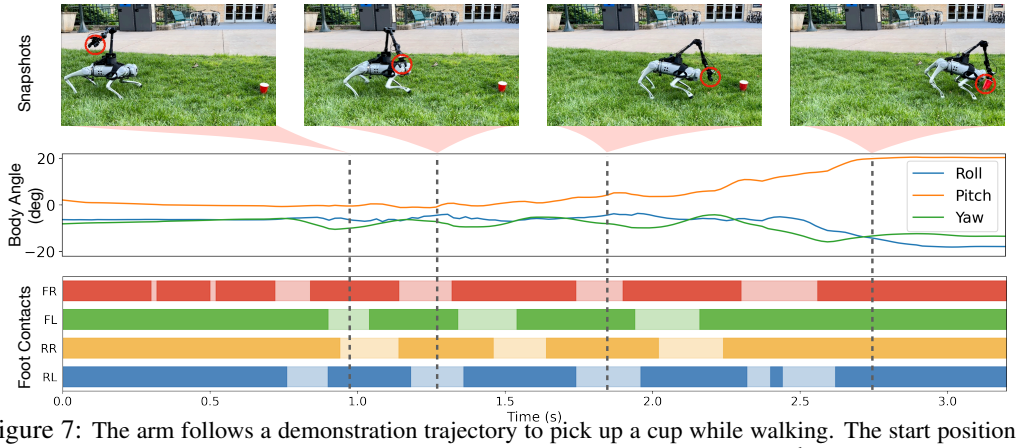

Figure 7: The arm follows a demonstration trajectory to pick up a cup while walking. The start position is $p = (0.5, -0.5, -1.2)$, at the right upper side of the robot and the end position is $p^{\text{end}} = (0.55, -0.9, 0.4)$, on the left lower front side close to the ground. $T_{\text{traj}} = 2.5s$. The robot initially stands on the ground and then is commanded a constant forward velocity $v_x^{\text{cmd}} = 0.35$. Meanwhile the end-effector position command starts to change. When the arm is not very low, the quadruped starts to walk without significant tilting behavior with a natural walking gait induced by energy consumption rewards. The darker color in Foot Contacts plot means foot has contact with the ground. As the arm moves lower, the quadruped starts to pitch down, roll to the left and yaw slightly to the right to help the arm reach the goal. Videos at https://maniploco.github.io/

follow in an open-loop manner while being commanded to walk at the same time. Our result shows stability, coordination and robustness on uneven grass terrains as shown in Figure 7.

4 Related Work

Legged Locomotion Traditional control-based methods for legged robots often require meticulously designed controller and are hard to transfer between robots [1, 2, 3, 4, 5, 31, 32, 33, 34, 35, 36, 6, 37]. The extra weight and movement of the robot arm on top of the legged robot will make such design process even more challenging. Recent advances in reinforcement learning enable legged robots to traverse challenging terrains and adapt to challenging environment dynamics [38, 24, 22, 39, 40, 41, 42, 43, 44, 45, 46, 47, 22, 17, 48, 49, 50]. However these works only focus on the locomotion part but few interactions by manipulation with the environment or objects are studied.

Mobile Manipulation Adding mobility to manipulation is studied in [51, 52, 53, 8, 54, 55]. Advances have been made in the field of biped humanoid [56, 57, 58]. More recently, [8] proposed using an MPC controller to track the desired end-effector position of a robot arm mounted on a quadruped robot with a RL-based locomotion controller to maintain balance. However, the controller is decoupled for legs (RL) and arm (model-based). In [55], large language models are used to guide a mobile robot to finish different tasks using arms. However the manipulation and mobility are also utilized in a decoupled step-by-step manner, where the two parts do not run in coordination.

5 Discussion and Limitations

We proposed a hardware setup as well as an algorithm to learn whole-body control of a legged robot with robotic arm. Our policy shows coordination between legs and arm while being able to control them in a dynamic manner. The method is trained fully in simulation and then transferred to the real-world using a learned adaptation strategy. We show the utility of our framework through teleoperation, visual tracking and open-loop control across several real-world tasks.

Limitations The robotic arm used in our legged manipulator setup has low-cost motors that are less reliable and not dynamic. Due to this, the end-effector control of the arm is not as smooth. Although, the algorithm is still able to learn a decently dynamic controller. There are several ways in which the current methodology could be extended, such as, learning visual control policies from the camera on the arm, climbing on the obstacle using front legs to pick something up on the table where arm can not reach, etc. We believe this paper provides a first step towards several of such future directions.

References

[1] H. Miura and I. Shimoyama. Dynamic walk of a biped. *IJRR*, 1984.

[2] M. H. Raibert. Hopping in legged systems—modeling and simulation for the two-dimensional one-legged case. *IEEE Transactions on Systems, Man, and Cybernetics*, 1984.

[3] H. Geyer, A. Seyfarth, and R. Blickhan. Positive force feedback in bouncing gaits? *Proceedings of the Royal Society of London. Series B: Biological Sciences*, 2003.

[4] K. Yin, K. Loken, and M. Van de Panne. Simbicon: Simple biped locomotion control. *ACM Transactions on Graphics*, 2007.

[5] K. Sreenath, H.-W. Park, I. Poulakakis, and J. W. Grizzle. A compliant hybrid zero dynamics controller for stable, efficient and fast bipedal walking on mabel. *IJRR*, 2011.

[6] M. Hutter, C. Gehring, D. Jud, A. Lauber, C. D. Bellicoso, V. Tsounis, J. Hwangbo, K. Bodie, P. Fankhauser, M. Bloesch, et al. Anymal-a highly mobile and dynamic quadrupedal robot. In *IROS*, 2016.

[7] L. Sentis and O. Khatib. A whole-body control framework for humanoids operating in human environments. In *Proceedings 2006 IEEE International Conference on Robotics and Automation, 2006. ICRA 2006.*, pages 2641–2648. IEEE, 2006.

[8] Y. Ma, F. Farshidian, T. Miki, J. Lee, and M. Hutter. Combining learning-based locomotion policy with model-based manipulation for legged mobile manipulators. *arXiv [cs.RO]*, Jan. 2022.

[9] C. D. Bellicoso, K. Krämer, M. Stäuble, D. Sako, F. Jenelten, M. Bjelonic, and M. Hutter. Alma-articulated locomotion and manipulation for a torque-controllable robot. In *2019 International Conference on Robotics and Automation (ICRA)*, pages 8477–8483. IEEE, 2019.

[10] S. Zimmermann, R. Poranne, and S. Coros. Go fetch!-dynamic grasps using boston dynamics spot with external robotic arm. In *2021 IEEE International Conference on Robotics and Automation (ICRA)*, pages 4488–4494. IEEE, 2021.

[11] N. Bernstein. The co-ordination and regulation of movements. *The co-ordination and regulation of movements*, 1966.

[12] M. L. Latash. The bliss (not the problem) of motor abundance (not redundancy). *Experimental brain research*, 217(1):1–5, 2012.

[13] M. Bruton and N. O'Dwyer. Synergies in coordination: a comprehensive overview of neural, computational, and behavioral approaches. *Journal of Neurophysiology*, 120(6):2761–2774, 2018.

[14] B. Dynamics. Spot Arm. https://www.bostondynamics.com/, 2019.

[15] Z. Chen. unitree. https://www.unitree.com/products/go1/. Accessed: 2022-6-11.

[16] S. Kataoka, S. K. S. Ghasemipour, D. Freeman, and I. Mordatch. Bi-manual manipulation and attachment via sim-to-real reinforcement learning. *arXiv preprint arXiv:2203.08277*, 2022.

[17] Z. Fu, A. Kumar, J. Malik, and D. Pathak. Minimizing energy consumption leads to the emergence of gaits in legged robots. In *CoRL*, 2021.

[18] G. B. Margolis, G. Yang, K. Paigwar, T. Chen, and P. Agrawal. Rapid locomotion via reinforcement learning. *arXiv preprint arXiv:2205.02824*, 2022.

[19] N. Rudin, D. Hoeller, P. Reist, and M. Hutter. Learning to walk in minutes using massively parallel deep reinforcement learning. In *Conference on Robot Learning*, pages 91–100. PMLR, 2022.

[20] I. Akkaya, M. Andrychowicz, M. Chociej, M. Litwin, B. McGrew, A. Petron, A. Paino, M. Plappert, G. Powell, R. Ribas, et al. Solving rubik's cube with a robot hand. *arXiv preprint arXiv:1910.07113*, 2019.

[21] J. Schulman, F. Wolski, P. Dhariwal, A. Radford, and O. Klimov. Proximal policy optimization algorithms. *arXiv:1707.06347*, 2017.

[22] A. Kumar, Z. Fu, D. Pathak, and J. Malik. RMA: Rapid Motor Adaptation for Legged Robots. In *RSS*, 2021.

[23] G. B. Margolis, T. Chen, K. Paigwar, X. Fu, D. Kim, S. bae Kim, and P. Agrawal. Learning to jump from pixels. In *5th Annual Conference on Robot Learning (CoRL)*, 2021.

[24] J. Lee, J. Hwangbo, L. Wellhausen, V. Koltun, and M. Hutter. Learning quadrupedal locomotion over challenging terrain. *Science robotics*, 2020.

[25] T. Miki, J. Lee, J. Hwangbo, L. Wellhausen, V. Koltun, and M. Hutter. Learning robust perceptive locomotion for quadrupedal robots in the wild. *Sci Robot*, 7(62):eabk2822, Jan. 2022.

[26] L. Weihs, U. Jain, I.-J. Liu, J. Salvador, S. Lazebnik, A. Kembhavi, and A. Schwing. Bridging the imitation gap by adaptive insubordination. *Advances in Neural Information Processing Systems*, 34, 2021.

[27] S. Levine, C. Finn, T. Darrell, and P. Abbeel. End-to-end training of deep visuomotor policies. *The Journal of Machine Learning Research*, 17(1):1334–1373, 2016.

[28] H. Wang and A. Banerjee. Bregman alternating direction method of multipliers. *Advances in Neural Information Processing Systems*, 27, 2014.

[29] WidowX 250 robot arm 6DOF - X-Series robotic arm. https://www.trossenrobotics.com/widowx-250-robot-arm-6dof.aspx. Accessed: 2022-6-11.

[30] E. Olson. AprilTag: A robust and flexible visual fiducial system. In *Proceedings of the IEEE International Conference on Robotics and Automation (ICRA)*, pages 3400–3407. IEEE, May 2011.

[31] A. M. Johnson, T. Libby, E. Chang-Siu, M. Tomizuka, R. J. Full, and D. E. Koditschek. Tail assisted dynamic self righting. In *Adaptive Mobile Robotics*. World Scientific, 2012.

[32] M. Khoramshahi, H. J. Bidgoly, S. Shafiee, A. Asaei, A. J. Ijspeert, and M. N. Ahmadabadi. Piecewise linear spine for speed–energy efficiency trade-off in quadruped robots. *Robotics and Autonomous Systems*, 2013.

[33] A. D. Ames, K. Galloway, K. Sreenath, and J. W. Grizzle. Rapidly exponentially stabilizing control lyapunov functions and hybrid zero dynamics. *IEEE Transactions on Automatic Control*, 2014.

[34] D. J. Hyun, J. Lee, S. Park, and S. Kim. Implementation of trot-to-gallop transition and subsequent gallop on the mit cheetah i. *IJRR*, 2016.

[35] M. Barragan, N. Flowers, and A. M. Johnson. MiniRHex: A small, open-source, fully programmable walking hexapod. In *RSS Workshop*, 2018.

[36] G. Bledt, M. J. Powell, B. Katz, J. Di Carlo, P. M. Wensing, and S. Kim. Mit cheetah 3: Design and control of a robust, dynamic quadruped robot. In *IROS*, 2018.

[37] C. S. Imai, M. Zhang, Y. Zhang, M. Kierebinski, R. Yang, Y. Qin, and X. Wang. Vision-guided quadrupedal locomotion in the wild with multi-modal delay randomization. *arXiv:2109.14549*, 2021.

[38] J. Hwangbo, J. Lee, A. Dosovitskiy, D. Bellicoso, V. Tsounis, V. Koltun, and M. Hutter. Learning agile and dynamic motor skills for legged robots. *Science Robotics*, 2019.

[39] Z. Li, X. Cheng, X. B. Peng, P. Abbeel, S. Levine, and others. Reinforcement learning for robust parameterized locomotion control of bipedal robots. *arXiv preprint arXiv*, 2021.

[40] X. B. Peng, E. Coumans, T. Zhang, T.-W. E. Lee, J. Tan, and S. Levine. Learning agile robotic locomotion skills by imitating animals. In *RSS*, 2020.

[41] W. Yu, J. Tan, C. K. Liu, and G. Turk. Preparing for the unknown: Learning a universal policy with online system identification. In *RSS*, 2017.

[42] W. Yu, C. K. Liu, and G. Turk. Policy transfer with strategy optimization. In *ICLR*, 2018.

[43] W. Zhou, L. Pinto, and A. Gupta. Environment probing interaction policies. In *ICLR*, 2019.

[44] W. Yu, V. C. V. Kumar, G. Turk, and C. K. Liu. Sim-to-real transfer for biped locomotion. In *IROS*, 2019.

[45] W. Yu, J. Tan, Y. Bai, E. Coumans, and S. Ha. Learning fast adaptation with meta strategy optimization. *RA-L*, 2020.

[46] X. Song, Y. Yang, K. Choromanski, K. Caluwaerts, W. Gao, C. Finn, and J. Tan. Rapidly adaptable legged robots via evolutionary meta-learning. In *IROS*, 2020.

[47] I. Clavera, A. Nagabandi, S. Liu, R. S. Fearing, P. Abbeel, S. Levine, and C. Finn. Learning to adapt in dynamic, real-world environments through meta-reinforcement learning. In *ICLR*, 2019.

[48] L. Smith, J. C. Kew, X. B. Peng, S. Ha, J. Tan, and S. Levine. Legged robots that keep on learning: Fine-tuning locomotion policies in the real world. In *ICRA*, 2022.

[49] R. Yang, M. Zhang, N. Hansen, H. Xu, and X. Wang. Learning vision-guided quadrupedal locomotion end-to-end with cross-modal transformers. In *ICLR*, 2022.

[50] Z. Fu, A. Kumar, A. Agarwal, H. Qi, J. Malik, and D. Pathak. Coupling vision and proprioception for navigation of legged robots. In *Proceedings of the IEEE/CVF Conference on Computer Vision and Pattern Recognition*, pages 17273–17283, 2022.

[51] C. Sun, J. Orbik, C. M. Devin, B. H. Yang, A. Gupta, G. Berseth, and S. Levine. Fully autonomous real-world reinforcement learning with applications to mobile manipulation. In *Conference on Robot Learning*, pages 308–319. PMLR, 2022.

[52] J. Wong, A. Tung, A. Kurenkov, A. Mandlekar, L. Fei-Fei, S. Savarese, and R. Martín-Martín. Error-Aware imitation learning from teleoperation data for mobile manipulation. Dec. 2021.

[53] D. Honerkamp, T. Welschehold, and A. Valada. Learning kinematic feasibility for mobile manipulation through deep reinforcement learning. Jan. 2021.

[54] X. Ding and F. Yang. Study on hexapod robot manipulation using legs. *Robotica*, 34(2): 468–481, Feb. 2016.

[55] M. Ahn, A. Brohan, N. Brown, Y. Chebotar, O. Cortes, B. David, C. Finn, K. Gopalakrishnan, K. Hausman, A. Herzog, D. Ho, J. Hsu, J. Ibarz, B. Ichter, A. Irpan, E. Jang, R. J. Ruano, K. Jeffrey, S. Jesmonth, N. J. Joshi, R. Julian, D. Kalashnikov, Y. Kuang, K.-H. Lee, S. Levine, Y. Lu, L. Luu, C. Parada, P. Pastor, J. Quiambao, K. Rao, J. Rettinghouse, D. Reyes, P. Sermanet, N. Sievers, C. Tan, A. Toshev, V. Vanhoucke, F. Xia, T. Xiao, P. Xu, S. Xu, and M. Yan. Do as I can, not as I say: Grounding language in robotic affordances. Apr. 2022.

[56] S. Kuindersma, R. Deits, M. Fallon, A. Valenzuela, H. Dai, F. Permenter, T. Koolen, P. Marion, and R. Tedrake. Optimization-based locomotion planning, estimation, and control design for the atlas humanoid robot. *Autonomous robots*, 40(3):429–455, 2016.

[57] G. Ficht and S. Behnke. Bipedal humanoid hardware design: A technology review. *Current Robotics Reports*, 2(2):201–210, 2021.

[58] M. de Waard, M. Inja, and A. Visser. Analysis of flat terrain for the atlas robot. In *2013 3rd Joint Conference of AI & Robotics and 5th RoboCup Iran Open International Symposium*, pages 1–6. IEEE, 2013.